Robustness assessment of model-based control for the Archimedes Wave Swing

Duarte Valério, Pedro Beirão, Mário J. G. C. Mendes and José Sá da Costa

Abstract— **In this paper the robustness of three model-based control strategies—internal model control (IMC) with linear models, IMC with neural network models, and feedback linearisation control—for the Archimedes Wave Swing (AWS), a device designed to produce electricity from the energy of sea waves, is assessed by checking how their performance, optimised for a neutral tide with a standard atmospheric pressure, changes under high and low tides, and under atmospheric pressure variations. The original AWS controller and latching control are used as a term of comparison. Simulation results show that, as a rule, low tides and lower atmospheric pressures lead to higher power productions, while high tides and higher atmospheric pressures lead to lower power productions; but, in spite of model maladjustments, model-based control strategies are not at disadvantage when compared with latching control.**

I. INTRODUCTION

Wave energy converters (WECs) are devices that convert the kinetic and potential energy of sea waves into electricity. Several WECs, using different working principles and adapted to different locations and wave climates, are being developed so as to make use of this renewable form of energy, estimated to correspond to a worldwide power around 2 TW. One such device is the Archimedes Wave Swing (AWS), a prototype of which has been built and tested in Portugal (near Leixões, 5 km away from the coast, where it was 43 m under water) during 2004, and then, after the tests, decommissioned. A second-generation, improved prototype is currently under development.

To maximise energy production by the AWS, it is imperative that some suitable control strategy be employed. A comparison of simulation results for several possibilities is given in [1]. Published results, however, while taking into account differences between waves available in different months of the year, do not take into account water height variations due to tides, or atmospheric pressure changes due to weather conditions. Such changes (the one predictable, the other not) will affect the performance of control algorithms optimised for a situation with an average water height and a standard atmospheric pressure. In this paper, the robustness of the main control options available to such changes is assessed: section II presents models used; section III presents control strategies considered; section IV presents the results and offers comments.

Authors would like to thank AWS Ocean Energy Ltd. Research for this paper was partially supported by grant PTDC/EME-CRO/70341/2006 of FCT, funded by POCI 2010, POS C, FSE and MCTES; and by the Portuguese Government and FEDER under "Programa de Financiamento Plurianual das Unidades de I&D da FCT" (POCTI-SFA-10-46-IDMEC).

D. Valério and J. Sá da Costa are with IDMEC/IST, TULisbon, Av. Rovisco Pais 1, 1049-001 Lisboa, Portugal. duarte.valerio@ist.utl.pt, sadacosta@dem.ist.utl.pt

P. Beirão is with Instituto Superior de Engenharia de Coimbra, Dept. Mechanical Engineering, R. Pedro Nunes, 3030-199 Coimbra, Portugal. pbeirao@isec.pt

M. J. G. C. Mendes is with IDMEC / ISEL, Instituto Superior de Engenharia de Lisboa, R. Conselheiro Emídio Navarro, 1, 1959-007 Lisboa, Portugal. mmendes@dem.isel.ipl.pt

II. THE ARCHIMEDES WAVE SWING

The first-generation AWS is a point absorber WEC—that is to say, a WEC with a diameter neglectable when compared to a typical wave length—consisting in two main cylindrical and hollow parts, the floater and the silo, mounted in a structure to keep them together, with air and some sea water trapped within floater and silo (this space is called the central tank). The silo is fixed to the structure, and the structure in its turn is fixed to the sea-bottom; the floater is free to heave up and down, within the range of mechanical end-stops. This heave takes place because, when a wave crest passes over the AWS, the height of water increases, so does the pressure compressing the air within, and the floater moves down; and, when a wave trough passes over the AWS, the height of water decreases, so does the pressure, the air expands and the floater moves up. (This is depicted in Fig. 1.) The heaving motion of the floater is converted into electricity by an electrical linear generator (ELG) . Water dampers are mounted in the AWS structure, outside silo and floater, and become active when the floater gets close to the mechanical end-stops, providing an additional damping force, to prevent any strong collision.

A. Tides

As the tide changes, the average value of the height of the water column above the floater changes as well, and so the oscillations of the floater no longer are equidistant from the end-stops. To correct this, water pumps allow changing the volume of sea water inside the central tank, thus changing the average value of the air pressure therein. Since the tides are regular and can be accurately predicted (values can be obtained for Leixões, 41.1833° N, 8.7° W, using the XTide software [2]), such sea water volume changes can be scheduled with ease in advance. Simulations allowed adjusting the values in Table I. However, atmospheric pressure changes prevent this adjustment from being perfect (since all models assume a standard atmospheric pressure of $\overline{p_{atm}} = 101325$ Pa). Variations around $\overline{p_{atm}}$ of up to $\Delta p = 4000$ Pa (corresponding to severe high- or low-pressure systems) will be allowed for in what follows, leading to the nine cases listed in Table I.

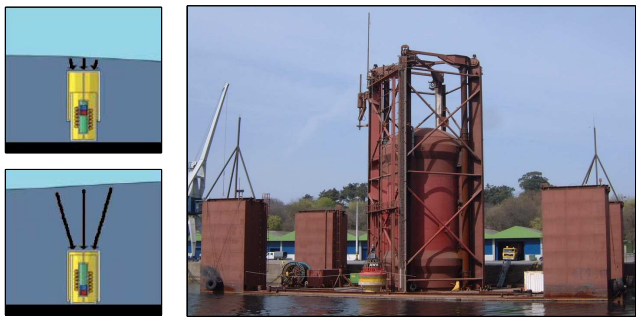

Fig. 1. The AWS working principle and the first prototype before submersion

TABLE I
TIDES AT THE AWS DEPLOYMENT SITE (1 Gg $= 10^6$ kg)

	Low tide	Neutral tide	High tide
Water height variation / m	-1.061	0	$+1.061$
Water in the central tank / Gg	1.0487	1.1275	1.1900
$p_{atm} = \overline{p_{atm}} - \Delta p$	case I	case IV	case VII
$p_{atm} = \overline{p_{atm}}$	case II	case V	case VIII
$p_{atm} = \overline{p_{atm}} + \Delta p$	case III	case VI	case IX

B. Wave models

Though real sea waves are not sinusoids, they can be decomposed as a sum of sinusoids, with a spectrum $S(\omega)$ giving the importance of the contribution of each frequency ω (in rad/s) [3]. Statistical data to characterise the wave climate in several locations in Portugal may be found with the ONDATLAS software [4]. The location available nearer to the AWS deployment site is Leixões–buoy, $41°12.2'$ N, $9°5.3'$ W. Table II gives three variables, for this location, for each of the months of the year, as well as for the entire year taken as a whole:

1) **The average significant wave height** H_s—The wave height is measured vertically from crest to trough. The average significant wave height is related to the spectrum by $H_s = 4\sqrt{\int_0^{+\infty} S(\omega)d\omega}$, and is the average height of the $\frac{1}{3}$ highest waves [5].
2) **Maximum values of the wave energy period** T_e—The energy period of an irregular wave of significant height H_s is, by definition, the period of a regular wave of (constant) height H_s that carries the same power [6], and is given by

$$T_e = \frac{\int_0^{+\infty} \frac{S(\omega)}{\omega} d\omega}{\int_0^{+\infty} S(\omega) d\omega} \quad (1)$$

3) **Minimum values of the wave energy period** T_e**.**

Throughout this paper, simulations are performed using irregular waves, corresponding to twelve sea states, one for each month of the year, generated using H_s values from Table II together with Pierson-Moskowitz's spectrum [5], that models the behaviour of real sea waves in the Northern Atlantic Ocean, and is given by (in SI units)

$$S(\omega) = \frac{A}{\omega^5} \exp\left(-\frac{B}{\omega^4}\right) \quad (2)$$

$$A = 0.780 \quad (3)$$

$$B = \frac{3.11}{H_s^2} \quad (4)$$

The sinusoids making up each irregular wave have random periods within the range of T_e in Table II[1].

It is clear that there are significant variations in wave characteristics along the year, and it will be useful to divide months according to the average energy content of waves, that depends on H_s. Periods when H_s is above or below average will be distinguished below by referring them, for expediency, as "summer" and "winter". "Summer" means the May–September period, when H_s is below its average value (during October H_s equals the average: it did not prove beneficial to consider October as being still "summer"); "winter" means the October–April period.

C. Nonlinear model of the AWS

Applying Newton's law to the floater, we get

$$f_{pi} - f_{hs} - f_{rad} + f_{exc} - w_f - f_n - f_v - f_m - f_{wd} - f_{lg} = m\ddot{\xi} \quad (5)$$

The floater's mass is m and its vertical acceleration is $\ddot{\xi}$. The force acting thereupon is the sum of the forces due to internal air pressure inside the central tank f_{pi}, to the hydrostatic impulse f_{hs}, to wave radiation f_{rad} (this being the force exerted on the AWS by the wave that the floater creates by its movement), to wave excitation f_{exc} (this being the force exerted on the AWS by the incident sea waves assuming that the floater is not moving), to the weight of the floater w_f, to a nitrogen cylinder extant inside the AWS f_n, to the hydrodynamic viscous drag f_v, to mechanical friction f_m, to the water dampers f_{wd}, and to the ELG f_{lg}. The last two are the forces we can control, and their sum will be called control force f_u. Since the water dampers are only sporadically used, most of the time $f_u = f_{lg} + f_{wd} \approx f_{lg}$ (though not when the floater gets close to the end-stops). In (5), positive values are given to the most natural direction; hence most forces point downwards. Small-case letters are being used for variables in the time-domain; their Laplace transforms (in the frequency domain) will be denoted using the corresponding capitals. (Hence $\Xi(s) \stackrel{\text{def}}{=} \mathcal{L}[\xi(t)]$, $F_{lg}(s) \stackrel{\text{def}}{=} \mathcal{L}[f_{lg}(t)]$, and so on.)

The expressions for most forces in (5) are nonlinear; they are given in [8]. They were implemented in a Simulink-based simulator of the AWS, the AWS Time-Domain Model (TDM), that was used for the simulations presented in this paper[2]. Data provided by this nonlinear model was also used to identify the other models in this section, since extant data from the prototype is scant and insufficient.

[1]The Bretschneider spectrum is a more general spectrum, given by (2) with different values of A and B. It depends from two different parameters (H_s and the frequency at which $S(\omega)$ has its maximum value). There are authors, such as Falnes [3], [7], that also use the name Pierson-Moskovitz spectrum to refer to the Bretschneider spectrum.

[2]When preparing this paper, several parameters and significant values of the model have been altered, due to industrial protection reasons. Consequently, results below should not be construed as indicative of the AWS first prototype actual performance, but they are significant as they reveal the robustness of the several control strategies.

TABLE II

CHARACTERISTICS OF SEVERAL IRREGULAR WAVES ACCORDING TO ONDATLAS

	Jan	Feb	Mar	Apr	May	Jun	Jul	Aug	Sep	Oct	Nov	Dec	Whole year
H_s / m	3.2	3.0	2.6	2.5	1.8	1.7	1.5	1.6	1.9	2.3	2.8	3.1	2.3
$T_{e,min}$ / s	5.8	5.8	5.2	5.5	5.0	4.7	4.6	5.0	5.2	5.3	5.5	5.3	4.6
$T_{e,max}$ / s	16.1	14.5	13.7	14.8	12.2	9.7	11.1	10.5	12.0	12.6	13.3	14.2	16.1

TABLE III

NEURAL NETWORK MODELS OF THE AWS

	Direct model	Inverse model
Inputs	f_{exc}, f_{lg}	f_{exc}, $\dot{\xi}$
Outputs	$\dot{\xi}$	f_{lg}
Type	Elman NN	Elman NN
Hidden layer	8 neurons	10 neurons
Activation	1st layer: $\tanh$	1st layer: $\tanh$
functions	2nd layer: linear	2nd layer: linear
Training	7 epochs	5 epochs

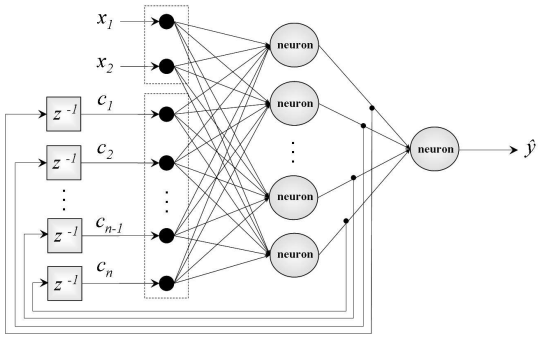

Fig. 2. Scheme of an Elman dynamic neural network

D. Linear model of the AWS

In spite of the significant nonlinearities present, from the description above the AWS can be expected to behave like a mass–spring–damper system. Applying Levy's identification method [9] to AWS simulation outputs, a second-order linear approximate model is found [10]:

$$\frac{\Xi(s)}{F_{exc}(s)+F_{lg}(s)} = \frac{2.259\times10^{-6}}{0.6324s^2+0.1733s+1} \qquad (6)$$

This model is valid for case V (see Table I). Parameters would be different if the identification had been performed with simulation results for any of the other eight cases.

E. Neural network (NN) models of the AWS

Having appeared as an attempt to find mathematical models of how the human nervous system works, and been found to be too simple for that, artificial NNs proved nevertheless able to model nonlinear plants, static or dynamic, providing useful black-box models. Algorithms were developed to train (that is, to adjust) the parameters of a NN according to a given collection of input-output data. The basics of NNs fall outside the scope of this paper; see for instance the references given below.

Among possible architectures for dynamic NNs [11], [12], it has been found [13] that the best for the AWS is the one known as locally recurrent network (LRN) models, using neurons arranged in layers (the last being the output layer and the others the hidden layers). In the simplest case there is only one hidden layer, to which NN inputs are fed; this layer's outputs are fed to the output layer, and are also delayed and fed back as NN inputs (known as context units). The output layer's outputs are the NN's outputs. Fig. 2 shows a LRN: x is the NN's input (here a 2-element vector), $\hat{y}$ is the NN's output (here a 1-element vector), n is the number of neurons in the hidden layer, and c denotes the context units. LRNs with only two layers, using activation functions $f(\zeta) = \tanh(\zeta)$ in the hidden layer and $f(\zeta) = \zeta$ in the output layer are called Elman NNs [14].

The backpropagation algorithm, together with Levenberg-Marquardt optimisation, was used as the NN training algorithm. Its performance depends heavily on the training data. The data should reflect all possible working conditions of the system. Too few data may be less than enough to train the NN properly. Too much data may overtrain it, so that it will just reproduce the training set and be unable to give meaningful outputs for new situations. It may also exhaust available memory, and cause numerical problems.

Direct and inverse NN models of the AWS were built using Matlab's Neural Network Toolbox. In such cases it may be useful to reuse input structures from existing linear models [11]. So, for the AWS direct model, the wave excitation force f_{exc} and the force exerted by the ELG f_{lg} were selected as inputs, and the floater's vertical velocity $\dot{\xi}$ as output. For the AWS inverse model, the inputs were f_{exc} and $\dot{\xi}$, and the output f_{lg}[3].

A 600 s wave corresponding to the parameters of the whole year was fed to the AWS TDM; the values of f_{exc}, f_{lg} and $\dot{\xi}$ obtained were used to train the NNs (see details in [13], [15]). After some trial and error (sometimes necessary in similar cases), the NNs with the characteristics given in Table III were chosen.

III. CONTROL STRATEGIES

In this paper three model-based control strategies are considered: internal model control using linear models, internal model control using NN models, and feedback linearisation. As a term of comparison, two control strategies not based upon an AWS model were employed: the original proportional controller developed for the AWS, and latching control. Such a comparison is important since these two control strategies might be expected to be more robust than model-based control strategies, exactly because they do not make

[3]Strictly speaking, the inverse model obtained is a partial inverse model, since f_{exc} is always considered an input. This was done because it is not created by the AWS: it is better viewed as a perturbation.

use of a model that may be inadequate when parameters change. Furthermore, latching control is important by itself as it combines simplicity with efficiency and is consequently of widespread use with WECs.

A. The original AWS controller

If the floater is left heaving freely, the ELG still exerts a residual force, from which some electricity is produced. But this situation without any control is clearly undesirable. Thus a controller was provided for the AWS prototype, exerting a control force f_u given by

$$|f_u(t)| = \left|\dot{\xi}(t)\right| k_p \left|\dot{\xi}(t) - \dot{\xi}_{stpl}(t)\right| \quad (7)$$

$$\left|\dot{\xi}_{stpl}(t)\right| = \begin{cases} \frac{2\pi}{10} 3.5 \sqrt{1 - \left(\frac{\xi(t)}{3.5}\right)^2}, & \text{if } |\xi(t)| < 3.5 \text{ m} \\ 0, & \text{if } |\xi(t)| \geq 3.5 \text{ m} \end{cases} \quad (8)$$

In (7), $\dot{\xi}_{stpl}$ is a reference value for $\dot{\xi}$, and k_p is the gain of a proportional controller, given by $k_p = 5 \times 10^6$. Constant 3.5 m shows up in (8) because it is the position of the floater's end-stops. Constant 10 s shows up because it is a reasonable value for the period of an incoming wave.

B. Phase and amplitude control

It is possible to show [7] that a WEC with a dynamic behaviour described exactly by a second-order transfer function without zeros will maximise energy absorption if $\dot{\xi}$ is proportional to f_{exc}; in other words, these two variables must be in phase and their magnitudes must verify a certain proportion. The enforcement of these two conditions by a suitable controller is called *phase and amplitude control*. Since the AWS is nonlinear and (6) is just an approximation, phase and amplitude control is not necessarily optimum [10]. Indeed simulations have shown that modifying the proportionality constant even leads to a higher energy production. The resulting setpoint is given by

$$\dot{\xi}_{stp2}(t) = \frac{2.2}{\max\limits_{\tau \in [t-80, t[} |f_{exc}(\tau)|} f_{exc}(t) \quad (9)$$

Constant 2.2 appears because the nominal value for the floater's vertical velocity that the AWS should work with is 2.2 m/s [16]. The excitation force must be estimated from measurements: values from the last 80 s are assumed as representative; this time window was chosen from several simulations as the one leading to the best results.[4]

[4]All previously published results of AWS phase and amplitude control calculate this maximum off-line, before the simulation, taking into account all the values that will be used during the whole duration of the simulation. In other words, for simulations below, that last for 600 s, the maximum is obtained for $\tau \in [0, 600]$, and does not depend on t. This not only requires knowing in advance what these values will be—something that does not happen in reality—but may also lead to poorer performances, when wave amplitude varies significantly. For both reasons the strategy used in this paper is a clear improvement.

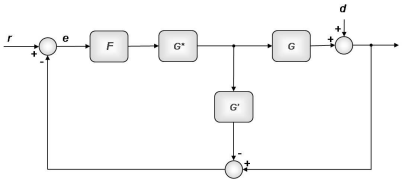

Fig. 3. Block diagram for Internal Model Control

C. Internal model control

The *internal model control* (IMC) methodology was used to make $\dot{\xi}$ follow setpoint $\dot{\xi}_{stp2}$. It makes use of the control scheme of Fig. 3 [17]. In that control loop, G is the plant to control, G' is a model of G, G^* is an inverse of G' (or at least a plant as close as possible to the inverse of G'), F is some judiciously chosen filter, r is the reference, d is a disturbance, and e is an error. If G' were exact, G^* were the exact inverse of G' (and hence also of G), and F were unity, we would have $e = r - d$: control would be perfect. Since no models are perfect, the error will not be exactly the disturbance. That is also why F exists and is usually a low-pass filter: to reduce the influence of high-frequency modelling errors. It also helps ensuring that product FG^* is realisable. Two types of AWS models were used to control the AWS TDM with IMC: 1) linear models and 2) NN models. When linear models were used [18], G' was (6) multiplied by s (this additional zero at the origin serving to have the floater's vertical velocity—and not its position—as the output), and $G^* = \frac{1}{G'}$. Since G^* is not causal, the filter F had to have more poles than zeros. It was found by trial and error that a second-order filter without zeros was the best option. The position of the poles was adjusted so as to maximise the absorbed wave energy for the simulation that uses an irregular wave with parameters corresponding to the month of March (deemed to be a significant month). The values found were

$$F = \frac{600}{(s+23)(s+20)} \quad (10)$$

This is reasonable since it corresponds to a low-pass filter that preserves the frequencies where waves are expected to appear, while cutting off higher ones. Because of this, the product FG^* has an integral action. Since e has a residual non-null average, this lead to an ever-increasing (or ever-decreasing) control action, something that was not intended. To prevent this, the control action had to be corrected, by subtracting its average, computed from the beginning of the simulation and actualised on-line. When NN models were used, all these control architecture options remained the same, allowing meaningful comparisons with the use of linear models.

D. Feedback linearisation

Feedback linearisation is a control strategy which aims to provide a control action judiciously chosen to cancel the nonlinear dynamics of the plant, so that the closed-loop dynamics will be (as much as possible) linear [19].

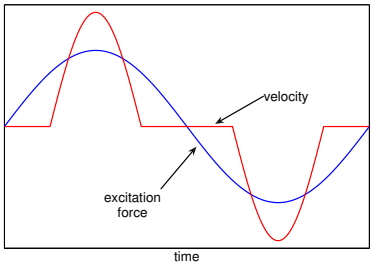

Fig. 4. Ideal evolution of the excitation force and of the floater's velocity with latching control

We assume that the ELG and the water dampers, which are to generate f_u, can respond immediately and without restrictions. This is really not the case (both devices saturate and have internal dynamics), but is an assumption good enough for our purposes. Hence

$$-f_u(t) = m\ddot{\xi}(t) - f_{pi}(t) + f_{hs}(t) + \\ + f_{rad}(t) - f_{exc}(t) + f_n(t) + f_v(t) + f_m(t) + w_f \quad (11)$$

Let us provide a control action given by

$$f_u(t) = f_{pi}(t) - f_{hs}(t) - f_{rad}(t) - f_n(t) - f_v(t) - \\ - f_m(t) - w_f - m\ddot{\xi}(t) + \dot{\xi}(t)\frac{\max_{\tau\in[t-80,t[}|f_{exc}(\tau)|}{2.2} \quad (12)$$

This is possible because there are explicit (nonlinear) expressions for all the forces involved in the right-hand side of (12). We will end up with a dynamic behaviour equal to (9) [1], [10].

In situations other than case V, the feedback linearisation controller was not given the new values for tide height and air pressure, but was kept working as though in case V. Even though the change in tide height might be predicted, this kept the controller simpler, and was a stronger test on its robustness.

E. Latching control

To have the floater's velocity in phase with the wave excitation force, *latching control* latches the floater when its velocity vanishes, and then releases it when it is predicted that its maximum (or minimum) velocity will coincide (in time) with the maximum (or minimum) of the wave excitation force. This is a highly nonlinear control strategy, that does not employ an amplitude setpoint for velocity. An ideal depiction of latching control is shown in Fig. 4. The floater of the AWS can be latched using both the ELG and the water dampers as follows. When the floater is latched, the duration of the last unlatched period is obtained. The next unlatched period is assumed to be going to last the same as the previous one. The floater's velocity is assumed to have its maximum (or minimum) precisely at the centre of that time interval. So the latching time is reckoned for that velocity maximum (or minimum) to coincide in time with the next maximum (or minimum) of the wave excitation force. The force required to latch the floater depends on the amplitude and period of the incoming wave, larger waves requiring a larger force and smaller waves requiring a smaller force. The forces for each wave amplitude and period are those necessary to latch effectively the floater when the incident wave is regular and has the required amplitude and period; suitable values were obtained beforehand with the AWS TDM for some regular waves, and then interpolated and extrapolated as needed. Other latching algorithms are possible, but the one above has given the best results together with the AWS TDM (see [10] for details).

IV. RESULTS AND COMMENTS

Simulation results are shown in Table IV. For case V, power extraction values are given[5]. For other cases, variations from the value of case V for the same month are given in percentage. Since cases and months are correlated (high pressures being more likely during summer and low pressures being more likely during winter), yearly averages may be misleading when $p_{atm} \neq \overline{p_{atm}}$, that is, in six out of the nine cases (I, III, IV, VI, VII and IX): for that reason, averages are given considering only summer months for cases I, IV and VII, and considering only winter months for cases III, VI and IX; averages for cases II, V and VII take into account the whole year. These averaged values are shown graphically in Figure 5. The results call for the following comments.

As a rule, low tides and lower atmospheric pressures lead to higher power productions, while high tides and higher atmospheric pressures lead to lower power productions. This is bad news for energy production during summer months, when higher atmospheric pressures are to be expected, but good news for energy production during winter months, when lower atmospheric pressures are to be expected. Since energy production is more significant during winter, this is likely to have an overall positive effect. These trends take place for all control strategies save latching, for which all deviations from case V induce a performance deterioration.

The most robust controller is the original, but this is of little use, since its performance is consistently very poor. The one that undergoes more variations is the feedback linearisation controller, which is also, by far, the best performing one; such variations are not large enough to threaten its overall best performance. Other control methods also undergo variations, all of comparable importance.

These results show that tides and atmospheric pressure variations affect significantly energy production, but that, in spite of model maladjustments, model-based control strategies are not at disadvantage when compared with latching, a control strategy not based upon a model.

Additional studies are needed to see if these control strategies, that may also be employed in other similar WECs, will then present similar robustness levels.

[5]These values do not match those previously published for the reasons given in footnote 4.

TABLE IV

FIGURATIVE DATA FOR POWER OBTAINED WITH IRREGULAR WAVES; CASE V: KW; OTHER CASES: PERCENTAGE OF CASE V FOR THE SAME MONTH

	case	Jan	Feb	Mar	Apr	May	Jun	Jul	Aug	Sep	Oct	Nov	Dec	Average (see text)
Original controller	I	112%	112%	112%	112%	110%	109%	109%	109%	110%	111%	112%	112%	112%
	II	103%	103%	102%	102%	102%	101%	101%	101%	102%	102%	103%	103%	102%
	III	101%	104%	108%	109%	112%	112%	113%	112%	111%	110%	106%	102%	112%
	IV	109%	109%	108%	108%	107%	106%	106%	106%	107%	107%	108%	108%	108%
	V	36.14	28.49	18.69	16.67	5.19	3.71	2.58	3.08	6.17	11.99	22.57	32.44	15.64
	VI	96%	96%	97%	97%	98%	98%	98%	98%	98%	97%	97%	96%	98%
	VII	100%	100%	100%	100%	100%	100%	100%	100%	100%	100%	100%	100%	100%
	VIII	95%	95%	96%	96%	97%	98%	98%	97%	97%	97%	96%	95%	96%
	IX	91%	92%	93%	93%	95%	95%	96%	95%	94%	94%	92%	92%	95%
IMC with linear models	I	127%	129%	130%	132%	125%	109%	107%	107%	118%	125%	123%	130%	128%
	II	113%	111%	111%	111%	106%	106%	104%	104%	109%	111%	109%	112%	109%
	III	92%	91%	92%	92%	92%	100%	100%	98%	94%	89%	91%	94%	97%
	IV	114%	115%	119%	116%	116%	105%	106%	107%	113%	117%	115%	114%	116%
	V	72.24	67.79	46.98	42.68	11.53	7.70	5.02	5.94	14.68	30.87	55.41	73.79	36.22
	VI	84%	84%	84%	85%	87%	93%	92%	92%	88%	83%	83%	85%	90%
	VII	97%	98%	98%	99%	101%	98%	100%	99%	100%	98%	99%	95%	98%
	VIII	84%	84%	85%	85%	88%	92%	92%	92%	88%	84%	84%	84%	87%
	IX	73%	73%	73%	73%	78%	85%	85%	85%	77%	72%	71%	74%	82%
IMC with NN models	I	103%	114%	123%	123%	111%	110%	109%	110%	111%	119%	145%	108%	119%
	II	118%	120%	114%	110%	102%	102%	102%	102%	102%	105%	128%	117%	110%
	III	86%	84%	90%	95%	111%	112%	112%	112%	110%	101%	87%	85%	111%
	IV	96%	107%	113%	115%	107%	107%	107%	107%	108%	111%	127%	100%	110%
	V	107.70	82.34	41.12	30.43	6.42	4.55	3.17	3.78	7.72	18.40	54.41	99.89	38.33
	VI	80%	78%	83%	86%	97%	98%	98%	98%	97%	91%	80%	78%	97%
	VII	93%	94%	98%	98%	100%	100%	100%	100%	100%	99%	95%	93%	96%
	VIII	81%	79%	84%	88%	97%	97%	97%	97%	96%	91%	81%	79%	89%
	IX	37%	63%	70%	76%	93%	95%	95%	94%	93%	83%	67%	63%	94%
Feedback linearisation	I	116%	115%	118%	113%	121%	121%	120%	122%	120%	120%	114%	117%	116%
	II	115%	115%	114%	115%	113%	114%	113%	114%	112%	113%	115%	115%	114%
	III	86%	83%	83%	83%	88%	89%	90%	89%	87%	84%	82%	85%	88%
	IV	97%	100%	105%	107%	115%	117%	116%	118%	113%	110%	101%	101%	103%
	V	99.75	83.03	59.82	55.63	21.23	15.99	11.44	13.01	24.25	42.01	70.01	92.13	49.03
	VI	78%	78%	77%	77%	79%	79%	81%	80%	78%	78%	76%	78%	79%
	VII	89%	91%	94%	94%	97%	97%	98%	98%	97%	95%	92%	90%	92%
	VIII	81%	81%	81%	81%	79%	79%	80%	79%	78%	80%	80%	81%	80%
	IX	62%	61%	62%	62%	62%	62%	64%	62%	61%	62%	61%	62%	62%
Latching	I	68%	63%	58%	63%	63%	63%	62%	61%	66%	65%	62%	66%	64%
	II	98%	100%	97%	100%	93%	90%	89%	88%	96%	98%	99%	98%	95%
	III	82%	82%	84%	84%	95%	98%	101%	99%	92%	88%	83%	82%	97%
	IV	77%	79%	78%	83%	84%	80%	80%	79%	87%	82%	77%	79%	79%
	V	90.33	81.00	59.44	55.78	20.44	14.64	9.35	11.97	23.78	42.05	68.02	80.70	46.46
	VI	87%	86%	88%	89%	96%	100%	103%	101%	93%	91%	87%	88%	98%
	VII	89%	91%	93%	94%	99%	99%	101%	100%	99%	96%	92%	93%	93%
	VIII	95%	93%	94%	94%	98%	101%	103%	101%	95%	95%	94%	97%	97%
	IX	79%	77%	79%	79%	87%	91%	96%	93%	84%	81%	78%	80%	90%

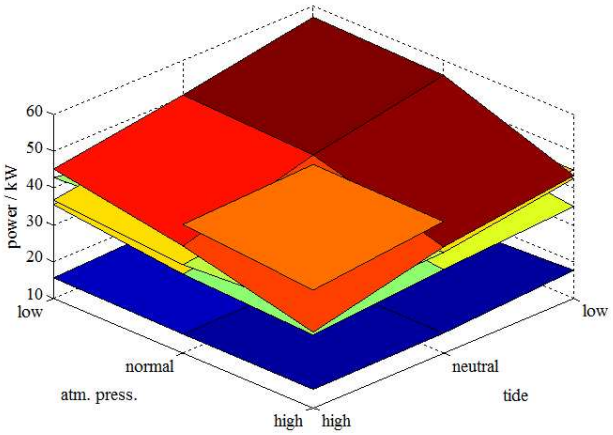

Fig. 5. Surface plots of the last column of Table IV; the layers correspond, from bottom to top, to the following control strategies: original controller, IMC with linear models; IMC with NN models; latching control (piercing through the upper surface for case VII); and feedback linearisation

REFERENCES

[1] D. Valério, P. Beirão, M. J. G. C. Mendes, and J. Sá da Costa, "Comparison of control strategies performance for a Wave Energy Controller," in *16th IEEE Mediterranean Conference on Control and Automation*, Ajaccio, 2008.

[2] http://www.mobilegeographics.com:81, Accessed May 2008.

[3] J. Falnes, "A review of wave-energy extraction," *Marine Structures*, vol. 20, pp. 185–201, 2007.

[4] M. T. Pontes, R. Aguiar, and H. Oliveira Pires, "A nearshore wave energy atlas for Portugal," *Journal of Offshore Mechanics and Arctic Engineering*, vol. 127, pp. 249–255, August 2005.

[5] W. H. Michel, "Sea spectra revisited," *Marine Technology*, vol. 36, no. 4, pp. 211–227, Winter 1999.

[6] "Performance assessment for wave energy conversion systems in open sea test facilities," The European Marine Energy Centre," Draft Standard, 2004.

[7] J. Falnes, *Ocean waves and oscillating systems*. Cambridge: Cambridge University Press, 2002.

[8] J. Sá da Costa, A. Sarmento, F. Gardner, P. Beirão, and A. Brito-Melo, "Time domain model of the Archimedes Wave Swing wave energy converter," in *Proceedings of the 6th European Wave and Tidal Energy Conference*, Glasgow, 2005, pp. 91–97.

[9] D. Valério, M. D. Ortigueira, and J. Sá da Costa, "Identifying a transfer function from a frequency response," *Journal of Computational and Nonlinear Dynamics*, vol. 3, no. 2, p. 021207, 2008.

[10] D. Valério, P. Beirão, and J. Sá da Costa, "Optimisation of wave energy extraction with the Archimedes Wave Swing," *Ocean Engineering*, vol. 34, no. 17-18, pp. 2330–2344, 2007.

[11] M. Nørgaard, O. Ravn, N. K. Poulsen, and L. K. Hansen, *Neural networks for modelling and control of dynamic systems: a practitioner's handbook*. London: Springer-Verlag, 2003.

[12] S. Haykin, *Neural Networks—A Comprehensive Foundation*, 2nd ed. New Jersey, U.S.A.: Prentice Hall International, Inc, 1999.

[13] P. Beirão, M. J. G. C. Mendes, D. Valério, and J. Sá da Costa, "Control of the Archimedes Wave Swing using Neural Networks," in *7th European Wave and Tidal Energy Conference*, Porto, 2007.

[14] J. Elman, "Finding structure in time," *Cognitive Science*, vol. 14, pp. 179–211, 1990.

[15] D. Valério, M. J. G. C. Mendes, P. Beirão, and J. Sá da Costa, "Identification and control of the AWS using neural network models," *Applied Ocean Research*, vol. 30, no. 3, pp. 178–188, 2008.

[16] H. Polinder, M. Damen, and F. Gardner, "Linear PM generator system for wave energy conversion in the AWS," *IEEE Transactions on Energy Conversion*, vol. 19, no. 3, pp. 583–589, September 2004.

[17] T. Hägglund and K. Åström, "Automatic tuning of PID controllers," in *The control handbook*, W. S. Levine, Ed. Boca Raton: CRC Press, 1996, pp. 817–826.

[18] J. Sá da Costa, P. Beirão, and D. Valério, "Internal Model Control applied to the Archimedes Wave Swing," in *International Conference on Control Systems and Computer Science*, Bucharest, 2007.

[19] J. Slotine and W. Li, *Applied Nonlinear Control*. Englewood Cliffs: Prentice Hall, 1991.